Journal of Catalysis **198,** 187–194 (2001)
doi:10.1006/jcat.2000.3127, available online at http://www.idealibrary.com on IDEAL®

Characterization of Silver–Rhodium Bimetallic Nanocrystallites Dispersed on γ-Alumina

Shanmugam Yuvaraj, Shu-Chin Chow, and Chuin-Tih Yeh[1]

Department of Chemistry, National Tsing Hua University, Hsinchu, Taiwan 30043, Republic of China

Received May 25, 2000; revised November 22, 2000; accepted November 28, 2000; published online February 15, 2001

A monometallic 3.2 wt% Rh on Al_2O_3 is used to prepare a series of Ag–Rh/Al_2O_3 bimetallic samples with different silver molar fractions ($X_{Ag} = 0.00$–0.91). Prepared bimetallic samples are characterized by a combination of the techniques of hydrogen chemisorption, X-ray diffraction (XRD), and ^{2}H NMR. The irreversible hydrogen uptake of Ag–Rh/Al_2O_3 increases on an initial addition of Ag to Rh/Al_2O_3 ($X_{Ag} < 0.09$) but decreases on further increase in X_{Ag}. The observed variation in uptake trend is explained in terms of the formation of two alloy phases, i.e., rhodium-rich phase (Rh) and silver-rich phase (Ag), on the surface of the dispersed bimetallic crystallites. Overall, the observed alloying behavior of Ag is similar to that of Cu when they are added onto Rh/Al_2O_3. However, experimental data from Au–Rh/Al_2O_3 catalysts indicated a nonalloying nature between Au and Rh. Deuterium species adsorbed on bimetallic Ag–Rh/Al_2O_3 samples showed a single ^{2}H NMR peak, the chemical shift and linewidth of which changed with the molar fraction of silver. Observed variations in NMR peaks are attributed to a change in the surface composition of alloy crystallites as well as to a fast exchange of deuterium adsorbed on (Rh) and (Ag) phases.

© 2001 Academic Press

Key Words: **bimetallic Ag–Rh; hydrogen chemisorptions; deuterium NMR.**

1. INTRODUCTION

The increasing importance of bimetallic catalysts is due to the fact that they are slowly but firmly replacing monometallic catalysts in industrial reactions. For example, Pt reforming catalysts have been replaced mostly by either Pt/Re or other platinum-based bimetallics for improved activity, selectivity, and stability (1). Among bimetallic catalysts, VIII–IB alloy catalysts have considerable academic interest due to their electronic configurations. The unfilled valence *d* orbital causes the group VIII component of the alloy to be active toward hydrogenation but the IB component (IB metals) is inactive and serves as a diluent. The presence of group IB elements also imparts some resistance to sintering of metal particles and self-poisoning by carbonaceous residues (2).

[1] To whom correspondence should be addressed. Fax: 886-35-711082 and 886-3-5726047. E-mail: ctyeh@mx.nthu.edu.tw.

Rhodium alloyed with Cu has been used for catalyzing benzene hydrogenation, alkane hydrogenolysis, CO hydrogenation, and methane decomposition (3–6). In a previous study on Cu–Rh/Al_2O_3 (7), Cu–Rh bimetallics with various molar fractions of copper, $X_{Cu} = N_{Cu}/(N_{Rh} + N_{Cu})$, were prepared and characterized by ^{2}H NMR. Formation of two alloy phases, i.e., the rhodium-rich phase (Rh) with $X_{Cu} < 0.05$ and the copper-rich phase (Cu) with $X_{Cu} > 0.50$, over the surface of bimetallic crystallites was confirmed. Furthermore (8), the (Rh) phase was found to exhibit considerably higher activity toward benzene hydrogenation than both the monometal Rh and the (Cu) phases. In view of the above said two alloy phases on Cu–Rh crystallites, it is of interest to determine the effect of addition of other IB metals, viz., Ag and Au, to Rh on alumina.

Ag–Rh catalysts have been tested for CO hydrogenation, CO insertion, ethane and methylcyclopentane hydrogenolysis, and recently butadiene hydrogenation (9–13). Paryjczak *et al.* (14, 15) adopted H_2 chemisorption, temperature-programmed reduction (TPR) and oxidation (TPO) techniques to characterize Ag–Rh on Al_2O_3 catalyst and concluded that there is no strong interaction between Rh and Ag. Catalyst characterization of Ag–Rh/SiO_2 by X-ray diffraction (XRD) and X-ray photoelectron spectroscopy (XPS) (9, 10) suggested that part of the Ag formed separate crystallites and part of the Ag deposited on the Rh surface. Despite the above observations, Rouco and Haller (9) reported that Ag and Rh formed bimetallic clusters on silica support and that Ag tends to cluster into islands. However, TiO_2 support altered Ag–Rh energetics so that Ag deposited uniformly over the Rh surface (10, 12, 16). There are only two reports available in the literature on the Au–Rh system (4, 17). Nunez and Rouco (17) used Au–Rh catalyst for ethane hydrogenolysis and observed no interaction between Au and Rh.

The purpose of this work was to collect ample evidence of the alloying ability of Ag and Au with Rh through ^{2}H NMR. ^{2}H NMR has been used in this laboratory to study many alumina-supported Rh catalysts (18–21) such as Cu–Rh and Pd–Rh catalysts. The same ^{2}H NMR technique was used to probe Ag–Rh and Au–Rh alloy catalysts supported on alumina for the present work.

0021-9517/01 $35.00
Copyright © 2001 by Academic Press
All rights of reproduction in any form reserved.

2. EXPERIMENTAL

2.1. Sample Preparation

Monometallic samples of 3.2 wt% rhodium, 4.0 wt% silver, and 9.1 wt% gold were prepared through the incipient wetness method by impregnating dried γ-alumina (Merck, 110 $m^2\ g^{-1}$, BET surface area) support with the corresponding nitrate solution. The resulting pastes were dried for 4 h at 383 K and then calcined for 4 h at 673 K. Ag–Rh and Au–Rh bimetallic samples were prepared from the 3.2 wt% Rh/Al_2O_3 monometallic sample by impregnating IB metallic nitrate followed by drying and calcination. All monometallic samples are referred to by the weight percentage before the metal; for instance, 3.2 wt% monometallic Rh sample is denoted 3.2Rh. Bimetallic samples are given in Tables 1 and 2 as whole numbers of their mole fraction preceding the bimetal, for instance, 09Ag–Rh represents 0.09 mole fraction of Ag in Ag–Rh bimetal on alumina.

2.2. Sample Characterization

2.2.1. Hydrogen chemisorption. Isotherms of hydrogen adsorption were measured at 300 K using the volumetric technique. Prior to the adsorption measurement, each sample was pretreated with a 1-h hydrogen reduction at 573 K and 1-h evacuation at around 5×10^{-5} Torr at 573 K. The total uptake of hydrogen chemisorption was measured at 300 K after evacuation. Reversible uptake was the second uptake obtained from the chemisorbed sample after it had been evacuated for 20 min at 300 K.

2.2.2. X-Ray diffractogram measurements. X-ray diffraction patterns were made using a Shimadzu XD-5 diffractometer employing Cu$K\alpha$ radiation ($\lambda = 1.5404$ Å). Instrumental broadening was determined by a reference sample with copper filament.

TABLE 1

Physicochemical Data on Ag–Rh/Al_2O_3 Samples

Sample	Ag loading (wt%)	X_{Ag}	$F_{(Ag)}$	Hydrogen uptake, N_H^m (μmol g^{-1})			ν (kHz)	δ_{obs} (ppm)
				N_H^t	N_H^r	N_H^{ir}		
3.2Rh	—	0.00	—	116.6	68.0	48.6	2.00	−140.0
09Ag–Rh	0.33	0.09	0.00	123.9	65.6	58.3	2.14	−138.5
23Ag–Rh	1.01	0.23	0.04	99.6	60.7	38.9	2.34	−135.0
33Ag–Rh	1.65	0.33	0.15	72.9	46.2	26.7	2.96	−123.0
43Ag–Rh	2.53	0.43	0.24	60.7	34.0	26.7	2.80	−115.0
59Ag–Rh	4.83	0.59	0.57	46.2	28.9	18.3	2.62	−79.5
75Ag–Rh	10.06	0.75	0.85	30.1	19.4	10.7	1.98	−50.5
83Ag–Rh	16.38	0.83	0.96	20.1	11.6	8.5	1.56	−39.0
91Ag–Rh	22.59	0.91	1.00	—	—	—	1.45	−35.0
4.0Ag	4.0	1.0	—	3.6	1.5	2.1	—	—

TABLE 2

Physicochemical Data on Au–Rh/Al_2O_3 Samples

Sample	Au loading (wt%)	X_{Au}	Hydrogen uptake, N_H^m (μmol g^{-1})			δ_{obs} (ppm)
			N_H^t	N_H^r	N_H^{ir}	
3.2Rh	—	0.00	116.6	68.0	48.6	−142.0
05Au–Rh	0.32	0.05	115.3	67.8	47.5	−141.0
11Au–Rh	0.76	0.11	—	—	—	−135.0
23Au–Rh	1.83	0.23	102.6	58.8	43.8	−135.0
33Au–Rh	3.02	0.33	—	—	—	−127.0
52Au–Rh	6.64	0.52	95.4	56.3	39.1	−126.0
67Au–Rh	12.44	0.67	—	—	—	−128.0
75Au–Rh	18.37	0.75	95.3	56.1	39.1	−135.0
9.1Au	9.10	1.00	1.7	0.9	0.8	—

2.2.3. Deuterium NMR. After a reduction–evacuation pretreatment similar to the chemisorption study, a portion of each sample was sealed with deuterium gas (Matheson, 99.99% purity) under desired pressure (200 Torr) and trasferred to a Bruker MSL-300 spectrometer for ^2H NMR measurements. An operating frequency of 46.05 MHz at a 7.05-T magnetic field was used for all measurements. ^2H NMR spectra were obtained by employing a single 90° pulse with 7.6-μs width. A dead time of 30 μs between a pulse and an acquisition was given with a repetition time of 0.1 s. CH_3COOD/CH_3COOH solution was used as an external standard ($\delta = 0$ ppm) for chemical shift calibrations.

3. RESULTS AND DISCUSSION

3.1. Hydrogen Chemisorption

Figure 1 illustrates the total and reversible hydrogen uptakes on the 43 Ag–Rh bimetallic sample. The experimental hydrogen uptake (N_H) of both isotherms increases dramatically at low hydrogen pressure, but their slopes decrease with pressure and are very much minimized beyond a hydrogen pressure of 4 kPa. Extrapolation of the isotherm asymptotes to zero hydrogen pressure gives a monolayer uptake (N_H^m). The difference between N_H^m uptakes of reversible (N_H^r) and total (N_H^t) isotherms is the irreversible hydrogen uptake (N_H^{ir}).

N_H^{ir} uptakes (Table 1) have been used to estimate the dispersion of noble metallic crystallites through the stoichiometric equations

$$x\,H_2 + 2M^s \rightarrow 2M^s\text{–}H_x, \qquad [1]$$

where M^s represents metal atoms exposed on the surface of dispersed metal crystallites and x denotes the stoichiometry of hydrogen chemisorption at the monolayer adsorption. The stoichiometry is generally regarded as 1.0 for group VIII metals (Pt, Pd, Rh, etc.) with a partially filled d orbital in the valence electron shell, and becomes negligible

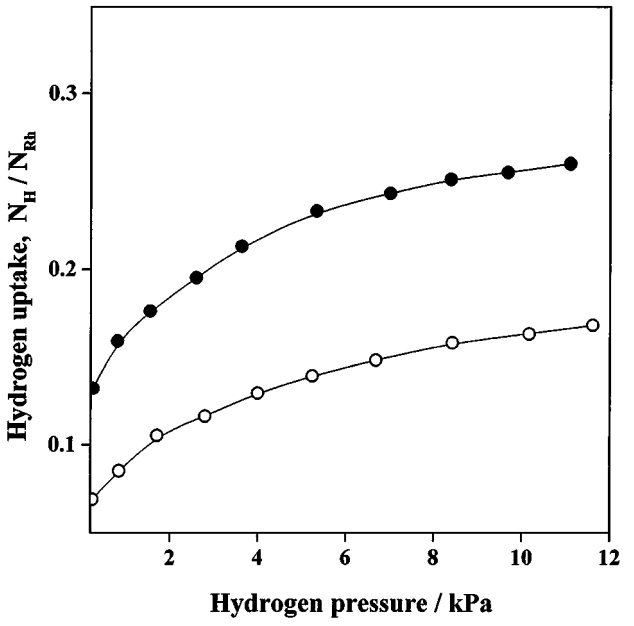

FIG. 1. Isotherms of hydrogen adsorption for 43Ag–Rh catalyst at 300K: ●, total uptake; ○, Reversible uptake.

(0.1 or less) for group IB metals (Cu, Ag, and Au) with a completely filled *d* orbital in the valence shell. Accordingly, the fraction of Rh atoms exposed to the crystallite surface (D_{Rh}) of IB–Rh alloys may be approximated by

$$D_{Rh} = N_H^{ir}/N_{Rh}, \quad [2]$$

where N_{Rh} is the number of Rh atoms in a sample. According to Fig. 1, the 43 Ag–Rh sample has a D_{Rh} of 0.12.

Figure 2 presents a series of total hydrogen uptake isotherms on the Ag–Rh catalysts prepared in this study. These bimetallic samples were prepared by impregnating different amounts of silver to several portions of the monometallic 3.2 wt% Rh/Al_2O_3. Uptake of $Ag–Rh/Al_2O_3$ bimetallic samples generally decreases with an increase in silver loading.This trend is conceivable from the knowledge that IB metals (Cu, Ag, and Au) do not strongly chemisorb hydrogen.Variations in N_H^{ir} of Ag–Rh samples were plotted in profile b of Fig. 3 against the bulk mole fraction of Ag in bimetallic samples, $X_{Ag} = N_{Ag}/(N_{Rh} + N_{Ag})$. The D_{Rh} of rhodium crystallites in the starting monorhodium sample ($X_{IB} = 0$) was around 32%. The N_H^{ir} of Ag–Rh bimetallic samples (profile b) generally decreases with X_{Ag}. Surprisingly, the 09Ag–Rh sample has a larger N_H^{ir} value than the monorhodium sample.

The increase in hydrogen uptake on alloying rhodium dispersed on Al_2O_3 with a small fraction of silver is not unique. This phenomenon has been reported in an initial addition of Ag to Rh/SiO_2 (9) and Cu to Rh/Al_2O_3 (7) (profile a in Fig. 3). As described in an earlier paper (7), addition of Cu to Rh/Al_2O_3 formed two alloy phases, (Rh) and (Cu), on the surface of bimetallic crystallites. (Rh) is a rhodium-rich

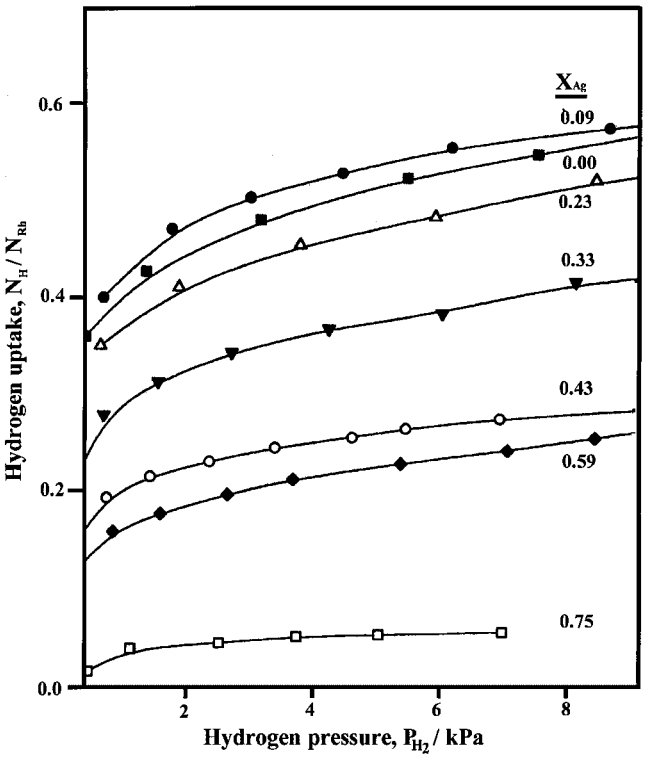

FIG. 2. Total hydrogen uptake isotherms for 3.2Rh ($X_{Ag} = 0.00$) and $Ag–Rh/Al_2O_3$ catalysts at 300 K.

phase with $X_{Cu} < 0.1$ and (Cu) is a copper-rich phase with $X_{Cu} > 0.50$. The composition of these two phases on the crystallite surface depends on the molar fraction of Cu added. (Rh) phase formed on initial addition of Cu

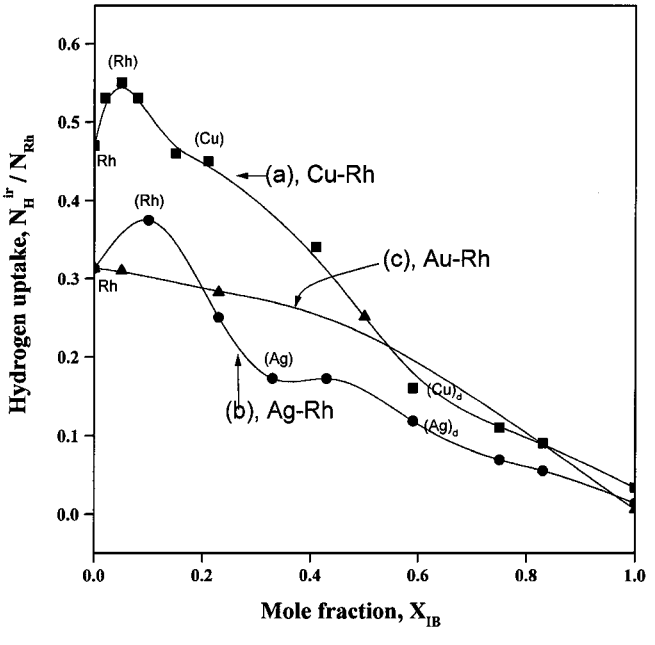

FIG. 3. Effect of Rh/Al_2O_3 alloying with IB metals on irreversible hydrogen uptake at 300 K.

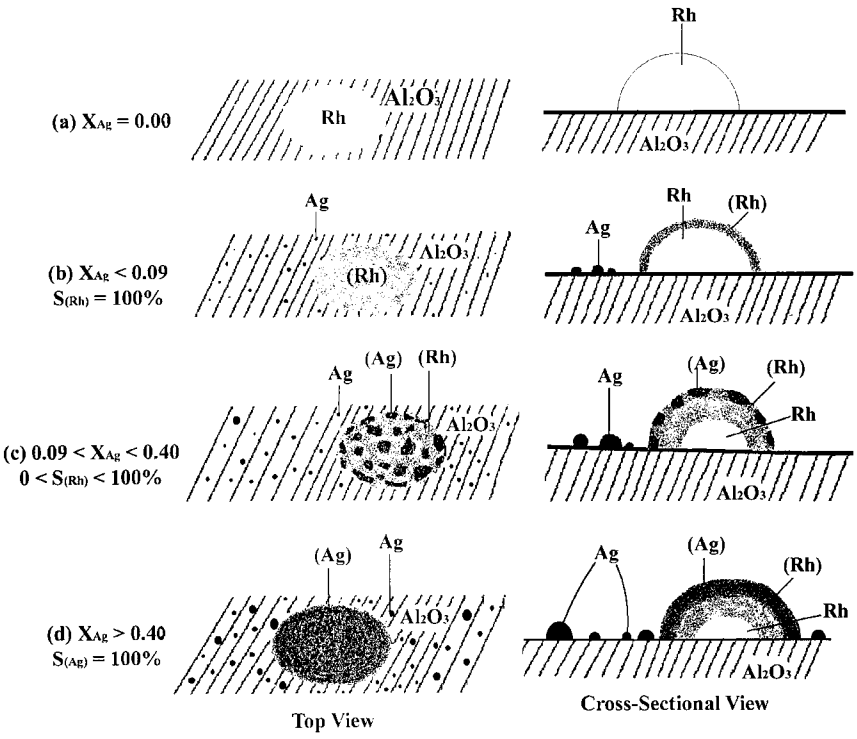

FIG. 4. Schematic diagram for the variation in distribution of different alloy phases on adding Ag to Rh/Al_2O_3. The relative size between particles of the Ag–Rh bimetallic and the monometallic silver is not in proportion. The bimetallic particle is purposely magnified to show the changes on the bimetallic surface with clarity.

to Rh/Al_2O_3 (7) was gradually replaced by (Cu) phase at high copper loading. The change in surface composition on adding Cu to Rh/Al_2O_3 is clearly seen in profile a of Fig. 3 and proceeds in three stages. In the first stage ($X_{Cu} < 0.05$), the pure Rh surface is converted to (Rh) phase. In the next stage ($X_{Cu} > 0.05$), the (Rh) on the surface is gradually replaced with (Cu) phase. As X_{Cu} is raised over 0.33, copper-diluted (Cu) phase, i.e., $(Cu)_d$, finally covered the surface. Hence, the increase in N_H^{ir} at $X_{Cu} = 0.05$ (profile a in Fig. 3) is attributed to formation of (Rh) phase on initial addition of Cu to Rh/Al_2O_3. The subsequent decrease in N_H^{ir} at $X_{Cu} > 0.05$ is due to the transformation of (Rh) phase into (Cu) and then to $(Cu)_d$, a copper-diluted (Cu) phase.

Following the explanation to $Cu–Rh/Al_2O_3$ (7), the variation in hydrogen uptake over $Ag–Rh/Al_2O_3$ (profile b in Fig. 3) can be explained by the formation of a rhodium-rich phase, (Rh), with $X_{Ag} < 0.10$; a mixture of (Rh) and (Ag), with $0.1 > X_{Ag} < 0.43$; and a silver-rich phase, (Ag), with $X_{Ag} > 0.43$ on the surface of bimetallic crystallites. The formation of (Rh) and (Ag) phases has already been suggested in their bimetallic bulk phase diagram (22). According to the bulk phase diagram, alloy phases of (Rh) ($X_{Ag} < 0.10$) and (Ag) ($X_{Ag} > 0.98$) may be formed on heating Ag and Rh together at 673 K.

Thus, the maximum N_H^{ir} value found in that profile b is directly correlated to the (Rh) phase on Ag–Rh bimetallic surface. The subsequent decrease in chemisorption on further addition of Ag is due largely to gradual replacement of (Rh) phase by (Ag) phase (when $X_{Ag} > 0.10$) and, finally, by silver-diluted (Ag) phase, $(Ag)_d$, with $X_{Ag} > 0.43$. From the present study, the molar compositional range of (Ag) phase is expanded from bulk phase, $X_{Ag} > 0.98$ to $X_{Ag} > 0.43$, for the dispersed bimetallic crystallites probably due to the highly miscible nature of nanoalloys. The variation of surface composition with X_{Ag} of $Ag–Rh/Al_2O_3$ is schematically described in Fig. 4.

As seen in profile c of Fig. 3, even though the hydrogen uptake of $Au–Rh/Al_2O_3$ mildly decreases on increasing the molar fraction of Au, the uptake is not significantly affected (also Table 2). Moreover, no significant uptake was observed on initial addition of Au to Rh/Al_2O_3 as found in profiles a and b after addition of copper and silver. This indicates that patches of gold partially cover the crystallites' surface but do not form an alloy phase with Rh. This result is in good agreement with the findings of Nunez and Rouco (17), who observed that the interaction between gold and rhodium is negligible in $Au–Rh/Al_2O_3$.

It is conceivable that addition of either a little Cu or a little Ag to Rh created new active sites from alloy formation (9, 11, 23–29). Both Cu and Ag cannot chemisorb hydrogen strongly because of filled *d* orbitals in their valence shell. According to Pauling's electronegativity scale, Cu and Ag are more electropositive (1.9 for both) than Rh (2.2). The

relatively electropositive nature of Cu and Ag metals causes a shift of their valence electronic cloud toward the vacant *d* orbitals of group VIII metal, Rh, during alloy formation. This shift may cause a partial vacancy in the valence *d* orbital of Cu and Ag and enhances their hydrogen chemisorption ability. But, the difference of Au (2.4) from Ag and Cu lies in its inability to transfer part of its electronic cloud toward vacant *d* orbitals of Rh to facilitate the formation of alloy between Rh (2.2) and Au (2.4) elements.

Further, surface energy also played a vital role in bringing down the hydrogen chemisorption ability of Rh on addition of IB metals. Group IB metals generally have a lower (22, 30) surface energy (1.35, 1.10, and 1.40 J m^{-2} for Cu, Ag, and Au respectively) compared with Rh (2.00 J m^{-2}) and, hence, tend to stay on the surface of Rh. As long as the mole fractions of Ag and Cu are at a minimum ($X_{IB} < 0.1$), they alloy with the surface rhodium to form (Rh) phase. When X_{Ag} is large enough, (Ag) or $(Ag)_d$ phase dominates on the surface and causes the decrease in hydrogen chemisorption (Fig. 3).

3.2. *X-Ray Diffractograms*

X-Ray diffractograms of Ag–Rh and Au–Rh samples supported on Al_2O_3 are shown in Fig. 5. From Fig. 5, it is very difficult to observe the Rh(111) diffraction peak of the 3.2Rh sample with such a high dispersion of Rh ($D_{Rh} = 0.32$). A broad peak around 45.0° is caused by the support, γ-Al_2O_3, when dispersion of Ag–Rh becomes low. To serve the purpose of assessing the peak position of Rh reflection, a highly loaded 23% monometallic Rh/Al_2O_3 sample was prepared. The (111) diffraction peak of that sample is observed at 41.2° (not shown in Fig. 5). Silver and gold monometallic samples prepared in a similar way showed (111) peaks at 37.7° and 38.1°, respectively. It is expected that a homogeneous alloy between Rh and a group IB metal should vary with X_{IB} and display a diffraction peak in compliance with the theoretical relationship

$$2\theta = 2\theta_{Rh}(1 - X_{IB}) + 2\theta_{IB}X_{IB}. \quad [3]$$

The (111) diffraction peak of Ag–Rh alloy catalysts was found in Fig. 5 at 37.9°, 38.4°, and 38.7° instead of 38.3°, 39.1°, and 40.1° for the silver mole fractions (X_{Ag}) of 0.83, 0.59, and 0.09, respectively, in Ag–Rh bimetallics. The deviations may be attributed to an enrichment of Ag in the bimetallic phase. However, it is quite unclear whether the peaks are really from an alloy phase or from deposited Ag especially when the X_{Ag} value exceeds 0.59 in the sample. Nevertheless, the shift in the peak position of alloy samples suggests a change in surface composition from (Rh) phase to (Ag) or $(Ag)_d$ on increase of silver content. As mentioned in the earlier paper (7), Cu–Rh/Al_2O_3 catalysts showed a definitive alloy peak in Cu–Rh bimetallic samples and XRD was shown to be substantial evidence of the formation of alloy phases.

All gold samples showed only Au(111) diffraction peaks irrespective of its molar composition in the sample. This observation confirmed the nonalloying nature of Au with Rh, as found in chemisorption data. The variation of bimetallic surface with respect to molar fraction of gold added to Rh/Al_2O_3 is depicted in Fig. 6. An initial addition of Au formed scattered Au particles on Rh/Al_2O_3. But further

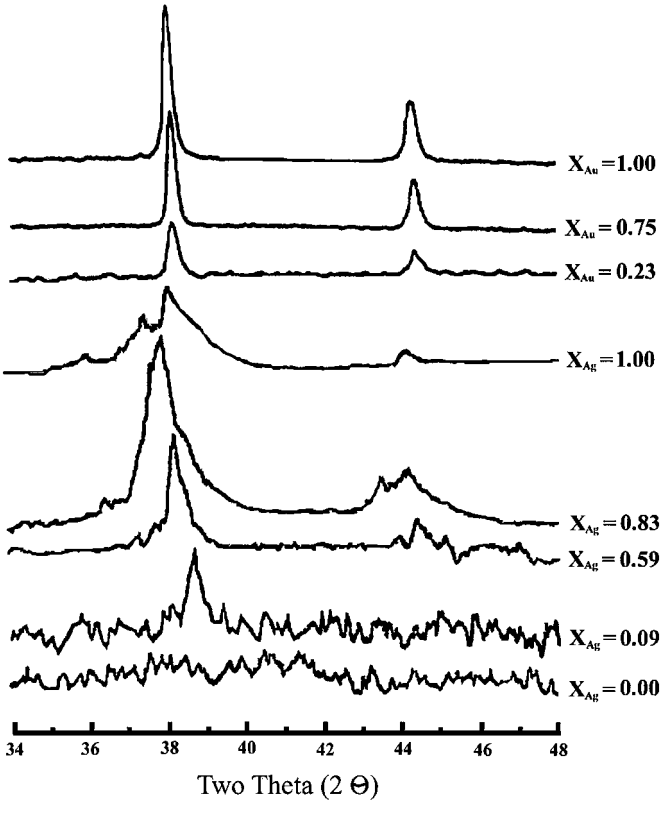

FIG. 5. X-Ray diffractograms of 3.2Rh ($X_{Ag} = 0.00$), Ag–Rh and Au–Rh/Al_2O_3 samples.

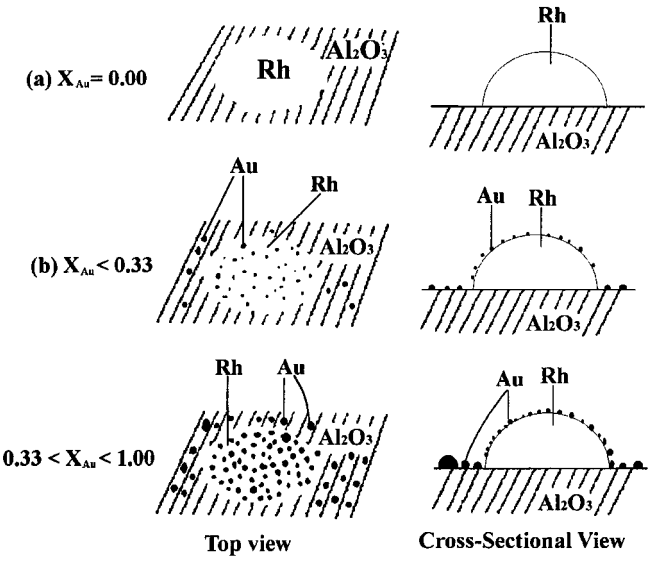

FIG. 6. Schematic diagram for the variation on adding Au to Rh/Al_2O_3.

increases in gold fraction, partially covered the rhodium surface with an increased amount of gold particles on the surface.

3.3. ^2H NMR

^{2}H NMR experiments were carried out on deuterium-adsorbed Ag–Rh catalysts with a deuterium overpressure of $P_{D_2} = 26.7$ kPa and the spectra obtained are shown in Fig. 7. The chemical shift of all spectra is referenced to deuteriums in CH_3COOD. No peak is observed at $\delta = 0$ ppm that corresponds to spilled over hydrogen onto Al_2O_3 but this peak has been reported over other supports such as SiO_2, TiO_2, and $SrTiO_3$ (31–33). The spectrum with $X_{Ag} = 0$ in Fig. 7 gave a signal at $\delta_{obs} = -140$ ppm and a peak width of $\Delta\nu = 2.00$ kHz. The upfield shift compared with the deuteriums in CH_3COOD ($\delta = 0$) is due to a shift of the electronic cloud from a valence *d* orbital of rhodium

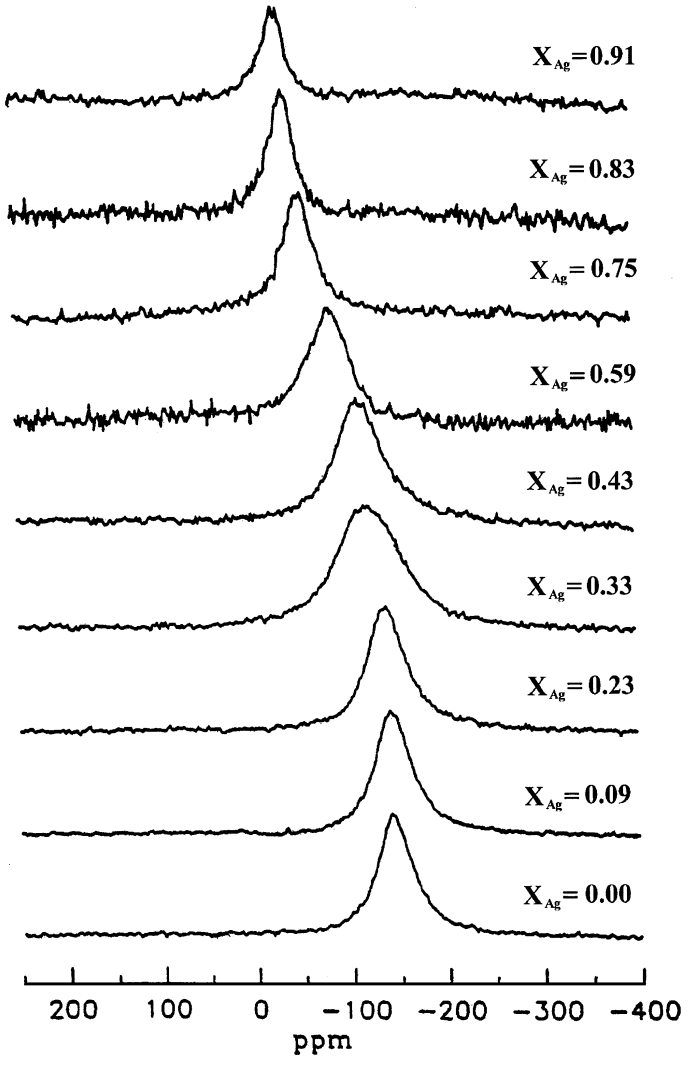

FIG. 7. ^{2}H NMR spectra of various Ag–Rh/ Al_2O_3 samples measured at 300 K and $P_{D_2} = 26.7$ kPa.

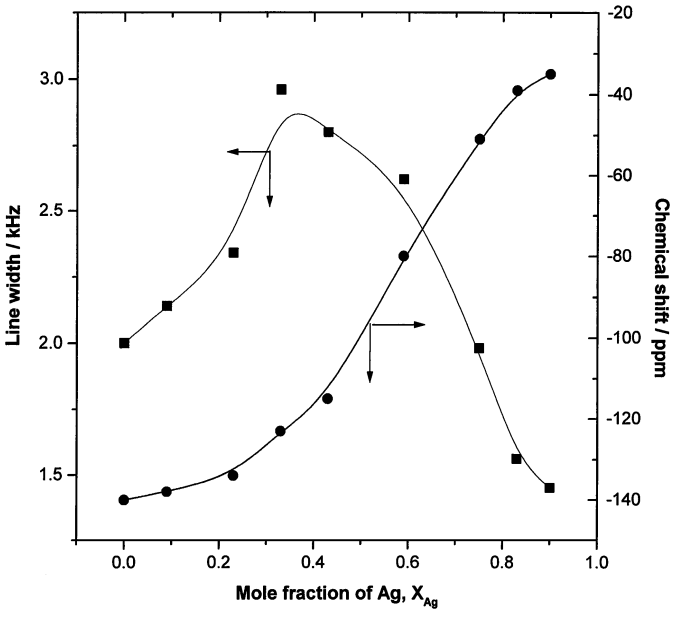

FIG. 8. Effect of Ag loading on chemical shift of deuterium adsorbed on Ag–Rh samples and linewidth at 300 K under deuterium pressure, $P_{D_2} = 26.7$ kPa.

atoms of dispersed crystallites toward adsorbed deuteriums (Knight shift).

^{2}H NMR spectra of deuterium-adsorbed Ag–Rh bimetallic samples varied with X_{Ag}. Observed variations in δ_{obs} and $\Delta\nu$ are plotted in Fig. 8. Addition of Ag to Rh/Al_2O_3 gradually downfielded the deuterium peak. Altogether, the observed downfield shift is attributed to the gradual change in surface composition from Rh to (Rh), (Ag), and then $(Ag)_d$ phases on the surface of bimetallic crystallites. Obviously, adsorbed deuteriums undergo the following fast exchange reaction on (Rh) and (Ag) phases:

$$(Rh)\text{–}H_\alpha + (Ag)\text{–}H_\beta \leftrightarrow (Rh)\text{–}H_\beta + (Ag)\text{–}H_\alpha. \quad [4]$$

A fraction of (Ag), $F_{(Ag)}$, formed on the surface of Ag–Rh bimetallic crystallites can be calculated from the observed chemical shift (δ_{obs}) of deuterium adsorbed on reduced catalysts through

$$\delta_{obs} = [1 - F_{(Ag)}]\delta_{(Rh)} + F_{(Ag)}\delta_{(Ag)}. \quad [5]$$

In Eq. [5], the chemical shift values of the (Ag) phase and (Rh) phase are -35 ppm ($X_{Ag} = 0.91$) and -138.5 ppm ($X_{Ag} = 0.09$), respectively. The surface of 91Ag–Rh catalyst ($X_{Ag} = 0.91$) consists of Ag diluted with (Ag) phase and hence the corresponding chemical shift value is taken as $\delta_{(Ag)}$ in Eq. [5]. Calculated $F_{(Ag)}$ values are listed in Table 1 and surpass X_{Ag} values if the bulk mole fraction of Ag in the bimetallic sample exceeds 0.59. This indicates surface enrichment in silver on increasing bulk mole fraction of silver in the bimetallic catalyst.

The $F_{(Ag)}$ values calculated from Eq. [5] for each sample are plotted in Fig. 9 against the linewidth obtained from Fig. 7. In the Ag–Rh/Al_2O_3 bimetallic system, an increase in linewidth from 2.00 kHz ($X_{Ag} = 0.0$) to the maximum of 2.96 kHz ($X_{Ag} = 0.33$) was observed at low X_{Ag}. Further additions of Ag on 33Ag–Rh catalyst narrowed the maximum linewidth to 1.45 kHz ($X_{Ag} = 0.91$), well below the linewidth of monometallic Rh/Al_2O_3. The much weaker adsorption of deuterium over $(Ag)_d$ of 91Ag–Rh sample compared with the Rh phase of monometallic sample caused a narrow linewidth on $X_{Ag} = 0.91$.

According to the theory of chemical exchange (7, 34), change in linewidth, $\Delta\nu[= (1/\pi T_{obs})]$ can be related to a observed spin–spin relaxation time (T_{obs}) of deuterium adsorbed on the Ag–Rh bimetallic sample as

$$1/T_{obs} = [1 - F_{(Ag)}]/T_{(Rh)} + F_{(Ag)}/T_{(Ag)} + 4\pi^2 [1 - F_{(Ag)}] \times F_{(Ag)}[\upsilon_{(Rh)} - \upsilon_{(Ag)}]^2 (k_1 + k_2)^{-1}, \quad [6]$$

where $T_{(Rh)}$ and $T_{(Ag)}$ are the spin–spin relaxation times of deuterium adsorbed on various (Rh) and (Ag) phase, respectively, in the absence of exchange. The linewidth values of deuterium on respective phases are denoted by $\upsilon_{(Rh)}$ and $\upsilon_{(Ag)}$ in hertz, and k_1, k_2 are the exchange rate constants of forward and backward exchange between (Rh) and (Ag) sites. A $(k_1 + k_2) = 2.4 \times 10^4\ s^{-1}$ was simulated for the rate constant of deuterium exchange at $T = 300$ K.

To confirm the exchange rate of deuterium on Ag–Rh catalysts, the calculated linewidths (from Eq. [6]) are plotted against the surface fraction of (Ag), $F_{(Ag)}$, in Fig. 9 (solid curve). Obviously, the simulated data points obtained from Eq. [6] match well the experimental data and a decent fitting of the curve indicates the exchange rate constant has a value of $2.4 \times 10^4\ s^{-1}$. The calculated constant is somewhat lower than that found (7) for Cu–Rh/Al_2O_3 ($= 4.73 \times 10^4\ s^{-1}$).

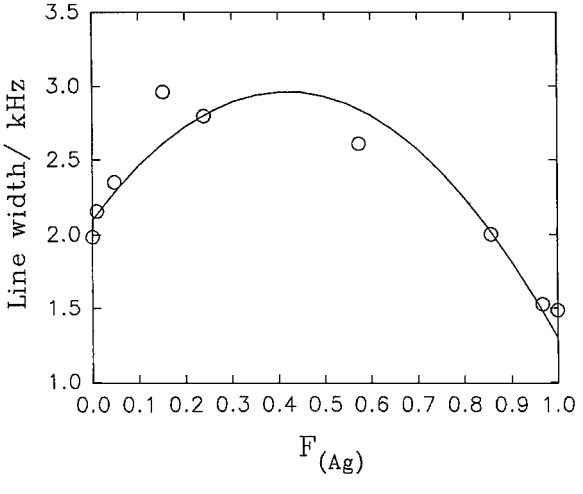

FIG. 9. Variation of $F_{(Ag)}$ with linewidth: simulated curve fitting (solid line, obtained from Eq. [6] over experimental data points (open circles).

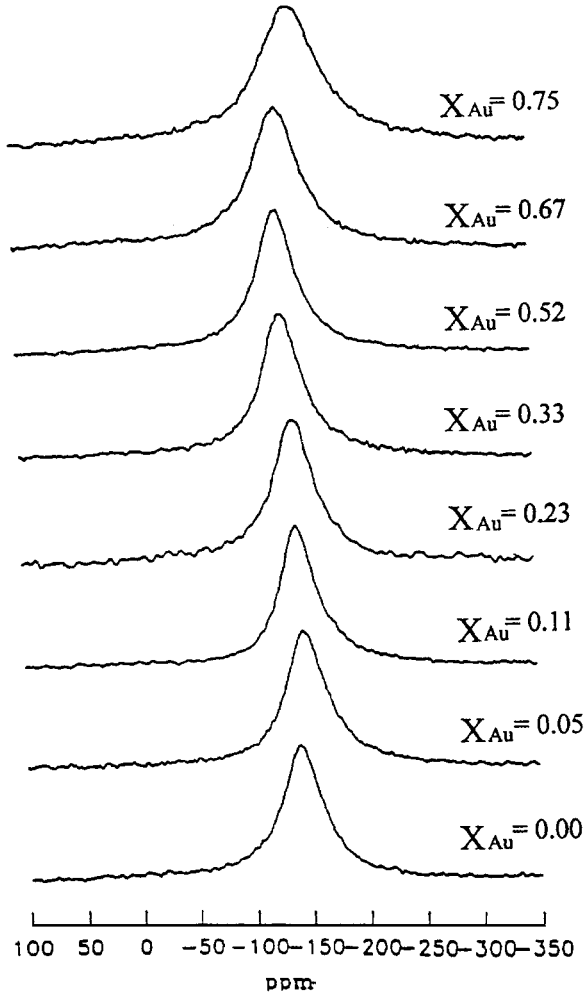

FIG. 10. ^2H NMR spectra of various Au–Rh catalysts measured at 300 K and $P_{D_2} = 26.7$ kPa.

On combining chemisorption with ^2H NMR and XRD results, it is evident that the surface of rhodium crystallites dispersed on Rh/Al_2O_3 is transformed from monometallic Rh to bimetallic (Rh) and then to (Ag) on adding Ag to Rh/Al_2O_3. This kind of trend has been reported for Cu–Rh/Al_2O_3 (7) and Ag–Ru/SiO_2 (28). However, from Fig. 10, neither the linewidth (about 2 kHz) nor the position of the deuterium peak (remained around −135 ppm) is significantly influenced by the addition of gold onto Rh/Al_2O_3. Hence, it may be concluded that Au alloys negligibly with Rh with any amount of addition at the nanoparticle level.

4. CONCLUSIONS

The following conclusions were derived from the present characterization study on Ag–Rh bimetallic alloy dispersed on alumina:

1. Addition of different fractions of silver to Rh/Al_2O_3 tends to form (Rh), (Ag), or a mixture of both (Rh) and

(Ag) alloy phases on the surface of metallic crystallites. A high capability for hydrogen uptake is observed on the initial additions of Ag. The increase in uptake reflects a flow of electronic cloud from Ag to Rh during the formation of alloy crystallites.

2. A single ^2H NMR peak is found from deuterium adsorbed on Ag–Rh/Al_2O_3 samples. Observed variations in chemical shift and linewidth are attributed to a consequential surface change on the alloy crystallites of Ag–Rh/Al_2O_3 and a fast exchange between deuterium atoms adsorbed on (Rh) and (Ag) phases.

3. The alloy formation of IB metals with Rh follows the trend Cu > Ag > Au. Gold particles may patch on the surface of nanosized rhodium dispersed on Al_2O_3 but no alloy formation was observed by either XRD or ^2H NMR.

ACKNOWLEDGMENT

The authors appreciate the National Science Council of the Republic of China for financial support for this study and a post-doctoral fellowship to S.Y.

REFERENCES

1. Jacobson, R. L., Kluksdahl, H. E., McCoy, C. S., and Davis, R. W., *Proc. Am. Pet. Inst. Div. Refin.* **49**, 504 (1969).
2. Clarke, J. K. A., *Chem. Rev.* **75**, 291 (1975).
3. Krishnamurthy, R., Chuang, S. S. C., and Ghosal, K., *Appl. Catal.* **114**, 109 ((1994).
4. Clarke, J. K. A., and Peter, A., *J. Chem. Soc. Faraday Trans. 1* **72**, 1201 (1975).
5. Coq, B., Dutartre, R., Figueras, F., and Rouco, A., *J. Phys. Chem.* **93**, 4904 (1989).
6. Shu, J., Grandjean, B. P. A., and Kaliaguine, S., *Appl. Catal. A* **119**, 305 (1994).
7. Chou, S. C., Yeh, C. T., and Chang, T. H., *J. Phys. Chem B* **101**, 5828 (1997).
8. Lu, C. M., Wang, I., Chou, S. C., and Yeh, C. T., submitted for publication.
9. Rouco, A. J., and Haller, G. L., *J. Catal.* **72**, 246 (1981).
10. Haller, G. L., Resasco, D. E., and Rouco, A. J., *Faraday Soc. Discuss.* **72**, 109 (1981).
11. Chuang, S. S. C., and Pien, S. I., *J. Catal.* **138**, 536 (1992).
12. Fenoglio, R. J., Nunez, G. M., and Resasco, D. E., *Appl. Catal.* **63**, 319 (1990).
13. Ksibi, Z., Ghorbel, A., and Bellamy, B., *J. Chim. Phys. Chim. Biol.* **94**, 1938 (1997).
14. Paryjczak, T., Goralski, J., and Jozwiak, K., *React. Kinet. Catal. Lett.* **16**, 111 (1981).
15. Paryjczak, T., Goralski, J., and Jozwiak, K., *React. Kinet. Catal. Lett.* **16**, 147 (1981).
16. Resasco, D. E., and Haller, G. L., *Appl. Catal.* **8**, 99 (1983).
17. Nunez, G. M., and Rouco, A. J., *J.Catal.* **111**, 41 (1988).
18. Chang, T. H., Cheng, C. P., and Yeh, C. T., *J. Chem. Soc. Faraday Trans.* **90**, 1157 (1994).
19. Chang, T. H., Chen, C. P., and Yeh, C. T., *J. Catal.* **138**, 457 (1992).
20. Chang, T. H., Chen, C. P., and Yeh, C. T., *J. Phys. Chem.* **96**, 4151 (1992).
21. Chang, T. H., Chen, C. P., and Yeh, C. T., *J. Phys. Chem.* **95**, 5239 (1991).
22. Karakaya, I., and Thompson, W. T., "Binary Alloy Phase Diagrams," ASM, Vol. 2, p. 1464 (1992).
23. Szanyi, J., and Goodman D. W., *J. Catal.* **145**, 508 (1994).
24. Zauwen, M. N., Crucq, A., Degols, L., Lienard, G., Frennet, A., Mikhalenko, N., and Grange, P., *Catal. Today* **5**, 237 (1989).
25. He, J. W., Kuhn, W. K., Leung, L. W. H., and Goodman, W., *J. Chem. Phys.* **93**, 7463 (1990).
26. Rodriguez, J. A., and Goodman, D. W., *J. Phys. Chem.* **95**, 4196 (1991).
27. Goodman, D. W., and Peden, C. H. F., *J. Chem. Soc. Faraday Trans 1* **83**, 1967 (1987).
28. Wu, X., Gerstein, B. C., and King, T. S., *J. Catal.* **121**, 271 (1990).
29. Rouco, A. J., Haller, G. L., Oliver, J. A., and Kemball, C., *J. Catal.* **84**, 297 (1983).
30. Anderson, J. R., and Preatt, K. C., "Introduction to Characterization and Testing of Catalysts." Academic Press, Sydney, 1985.
31. Uner, D. O., Pruski, M., and King, T. S., *J. Catal.* **156**, 60 (1995).
32. Sanz, J., and Rojo, M., *J. Phys. Chem.* **89**, 4974 (1985).
33. Sanz, J., Rojo, M., Malet, P., Munuera, G., Blasco, M. T., Conesa, J. C., and Soria, J., *J. Phys. Chem.* **89**, 5427 (1985).
34. Jackman, L. M., and Cotton, F. A., "Dynamic Nuclear Magnetic Resonanc." Wiley, New York, 1975.